Hindawi Publishing Corporation
EURASIP Journal on Wireless Communications and Networking
Volume 2008, Article ID 892193, 13 pages
doi:10.1155/2008/892193

Research Article

Reduced-Rank Shift-Invariant Technique and Its Application for Synchronization and Channel Identification in UWB Systems

Jian (Andrew) Zhang,[1,2] Rodney A. Kennedy,[2] and Thushara D. Abhayapala[2]

[1] *Networked Systems Research Group, NICTA, Canberra, ACT 2601, Australia*
[2] *Department of Information Engineering, Research School of Information Sciences and Engineering, The Australian National University, Canberra, ACT 0200, Australia*

Correspondence should be addressed to Jian (Andrew) Zhang, andrew.zhang@nicta.com.au

Received 31 March 2008; Revised 20 August 2008; Accepted 26 November 2008

Recommended by Chi Ko

We investigate reduced-rank shift-invariant technique and its application for synchronization and channel identification in UWB systems. Shift-invariant techniques, such as ESPRIT and the matrix pencil method, have high resolution ability, but the associated high complexity makes them less attractive in real-time implementations. Aiming at reducing the complexity, we developed novel reduced-rank identification of principal components (RIPC) algorithms. These RIPC algorithms can automatically track the principal components and reduce the computational complexity significantly by transforming the generalized eigen-problem in an original high-dimensional space to a lower-dimensional space depending on the number of desired principal signals. We then investigate the application of the proposed RIPC algorithms for joint synchronization and channel estimation in UWB systems, where general correlator-based algorithms confront many limitations. Technical details, including sampling and the capture of synchronization delay, are provided. Experimental results show that the performance of the RIPC algorithms is only slightly inferior to the general full-rank algorithms.

1. INTRODUCTION

Ultra-wideband (UWB) signals have very high temporal resolution ability. This implies a frequency-selective channel with rich multipath in practice. Identifying and utilizing this multipath is a must for achieving satisfactory performance in a UWB receiver. To estimate the numerous and closely spaced multipath signals in a UWB channel, high temporal resolution channel identification algorithms with low complexity are required for practical implementations.

Some related UWB research based on the traditional correlator techniques have been reported [1, 2]. The correlator-based techniques are simple, but they might confront many limitations in UWB systems. For example, they usually have limited resolution ability which largely depends on the number of samples, and to improve resolution, higher sampling rates are required; they are ineffective in coping with overlapping multipath signals; they are susceptible to interchip interference (ICI) and narrowband interference (they lack flexibility for removing narrowband interference); and with the number of multipaths increasing, the complexity of these algorithms increases rapidly. In [3], a frequency domain approach is introduced based on subspace methods. Although this scheme is derived from the authors' preceding work on the "sampling signals with finite rate of innovation," it is in essence the same as those in [4, 5] based on the well-known shift-invariant techniques [6, 7].

Shift-Invariant techniques, such as ESPRIT and its variants [8, 9], matrix pencil methods [10], and state space methods [6], are a class of signal subspace approaches with high resolution ability but relatively high computational complexity associated with the singular value decomposition (SVD) and generalized eigenvalue decomposition (GED). This associated high complexity makes these techniques less attractive in online implementations. To make the algorithms noise-stable, truncated data matrices are generally formed

using the SVD, and the original GED in a larger space is transformed into that in a relatively smaller space. This is an application of rank reduction techniques.

Rank reduction is a general principle for finding the right tradeoff between model bias and model variance when reconstructing signals from noisy data. Abundant research has been reported, for example, in [11–14]. Based on some linear models, these rank reduction techniques usually try to find a low-rank approximation of the original data matrix following some optimization criteria such as least squares or minimum variance. In the SVD-based reduced-rank methods, the low-rank approximation matrix is a result of keeping dominant singular values while setting insignificant ones to zero.

Although rank reduction is inherent in shift invariant techniques, in the literature, the rank reduction is only limited to separating the signal subspace and noise subspace, and the reduced rank is constrained to the number of signal sources, L, which is usually required to be known a priori or estimated online. Further reduction of the rank generally becomes a problem of signal space approximation by excluding weak signal subspaces. Then we ask, is it possible to reduce the rank to any p ($p < L$) using shift-invariant techniques supposing only p out of L signals (parameters) need to be estimated?

This reduction finds practical applications such as in the synchronization and channel identification of UWB signals. The UWB multipath channel is dense with L as large as 50 [15]. The general L-rank algorithms will have a high computational complexity in the order of 1.25×10^5 multiplications for $L = 50$. Although all multipath parameters can be determined, it is usually sufficient to know p ($p \ll L$) multipath with largest energy for the following reasons: (1) for the purposes of synchronization and detection, several multipath components are usually enough; (2) in the presence of noise, estimates cannot be accurate, and the estimates of multipath signals with lower energy contain relatively larger errors according to the Cramer-Rao bounds [16].

In this paper, we present some novel p-rank shift-invariant algorithms, and investigate their applications in joint synchronization and channel identification for UWB signals. These p-rank algorithms will be referred to as reduced-rank identification of principal components (RIPC) algorithms. Unlike general subspace methods, our schemes remove the constraint on L and p multipath signals with largest energy can be automatically tracked and identified, while the complexity can be significantly reduced by a factor related to p. The word "automatically" means that no further processing is needed to pick up p principal ones among more estimates. Actually, only p signals are estimated and they are supposed to be the principal ones. The value of p can be adjusted freely to meet different performance requirements of synchronization and specific multiple-finger receivers like RAKE .

The rest of this paper is organized as follows. In Section 2, the shift-invariant techniques are introduced. In Section 3, our new RIPC algorithms are derived using the harmonic retrieval model. In Section 4, the application of RIPC algorithms in the joint synchronization and channel estimation is presented. Technical details are given including sampling, deconvolution, FFT, and the capture of synchronization delay. Simulation results are given in Section 5. Finally, conclusions are given in Section 6.

The following notation is used. Matrices and vectors are denoted by boldface upper-case and lower-case letters, respectively. The conjugate transpose of a vector or matrix is denoted by the superscript $(\cdot)^*$, the transpose is denoted by $(\cdot)^T$, and the pseudoinverse of a matrix is denoted by $(\cdot)^\dagger$. Finally, $\mathbf{I}$ denotes the identity matrix and diag $(\cdots)$ denotes a diagonal matrix.

2. FORMULATION OF SHIFT-INVARIANT TECHNIQUES

Typical harmonic retrieval problems can be addressed as the identification of unknown variables from the following equation:

$$x(k) = \sum_{\ell=1}^{L} a_\ell e^{jk\omega_\ell} + n(k), \quad k \in [0, K-1], \tag{1}$$

where $j = \sqrt{-1}$ is the imaginary unit, $x(k)$ are the measured samples, $n(k)$ are the noise samples, K is the number of samples, a_ℓ and $\omega_\ell \in [0, 2\pi)$ are the unknown amplitudes and frequencies, to be determined.

Organize these measured samples $x(k)$ into an $M \times Q$ Hankel matrix $\mathbf{X}$ where the entries along the antidiagonals are constant, we get

$$\mathbf{X} = \begin{pmatrix} x(2) & x(3) & \cdots & x(Q+1) \\ x(3) & x(4) & \cdots & x(Q+2) \\ \vdots & \vdots & \ddots & \vdots \\ x(M+1) & x(M+2) & \cdots & x(K) \end{pmatrix}, \tag{2}$$

where $M + Q = K$, $\min(M, Q) \geq L$ and $\max(M, Q) > L$. The used samples usually start from $x(0)$. In order to make the notations in (4) applicable to subsequent equations, for example, (19), we start from $x(2)$ here. Without loss of generality, we assume $M \geq Q$. In the noise-free case, $\mathbf{X}$ can be factorized as

$$\mathbf{X} = \mathbf{F}_M \mathbf{A} \mathbf{F}_Q^T, \tag{3}$$

where

$$\begin{aligned} \mathbf{F}_M &= \mathbf{F}(M), \\ \mathbf{F}_Q &= \mathbf{F}(Q), \\ \mathbf{F}(m) &= [\mathbf{f}(m; \omega_1), \mathbf{f}(m; \omega_2), \ldots, \mathbf{f}(m; \omega_L)], \\ \mathbf{f}(m; \omega_\ell) &= [e^{j\omega_\ell}, e^{j2\omega_\ell}, \ldots, e^{jm\omega_\ell}]^T, \\ \mathbf{A} &= \text{diag}\,(a_1, a_2, \ldots, a_L). \end{aligned} \tag{4}$$

The Vandermonde matrix $\mathbf{F}(m)$ exhibits the so called *shift-invariant property*, that is,

$$\mathbf{F}(m)^{\uparrow d} = \mathbf{F}(m)_{\downarrow d} \mathbf{\Phi}^d, \tag{5}$$

where $d \geq 1$, $(\cdot)^{\uparrow d}$ and $(\cdot)_{\downarrow d}$ denote the operations of omitting the first d and omitting the last d rows of

a matrix, respectively, and $\mathbf{\Phi} = \text{diag}(e^{j\omega_1}, e^{j\omega_2}, \ldots, e^{j\omega_L})$ contains the desired frequencies. This property facilitates the development of various shift-invariant techniques. By constructing two L rank matrices $\mathbf{Y}_1$ and $\mathbf{Y}_2$ with the inherent shift-invariant property, the diagonal elements of $\mathbf{\Phi}$ can be obtained by solving the generalized eigenvalues of the matrix pencil $\{\mathbf{Y}_1 - \xi\mathbf{Y}_2\}$. These two matrices $\mathbf{Y}_1$ and $\mathbf{Y}_2$ can be constructed directly from $\mathbf{X}$ using $\mathbf{Y}_1 = \mathbf{X}_{\downarrow d}$ and $\mathbf{Y}_2 = \mathbf{X}^{\uparrow d}$, or from the correlation matrices of $\mathbf{X}$, or from the singular vectors of $\mathbf{X}$. The use of $d > 1$ can improve resolution ability and result in smaller variance of estimates, but d must be chosen to ensure $d < 2\pi/\max(\omega_\ell)$ in order to avoid phase ambiguities, and maintain $M - d \geq L$. In the presence of noise, the above solutions hold as approximations while the criterion of least squares or total least squares is applied [7].

Substituting estimated frequencies into (1), the amplitudes a_ℓ can be obtained by solving a Vandermonde system using least squares type algorithms [13, 17]. The energy of harmonics can also be solved according to the generalized eigenvectors (GVs) [8]. In either method, the accuracy of amplitude estimates is inferior to frequency estimates whose accuracy is guaranteed by the stability of the singular values in the presence of a perturbation matrix. The accuracy of amplitude estimates will sometimes contribute to the overall performance of estimation. For example, when we need to pick out several harmonics with largest energy among all estimates, the errors in amplitude estimates will influence the correctness of the selected harmonics significantly.

3. REDUCED-RANK IDENTIFICATION OF PRINCIPAL COMPONENTS (RIPC)

3.1. Generalization of the shift-invariant methods

The shift-invariant techniques can be interpreted from various angles, such as the subspace viewpoint [8, 9], the state space viewpoint [6], and the matrix pencil viewpoint [10]. We generalize a result in the viewpoint of matrix pencil below, which will be used in the subsequent development of the paper.

Proposition 1. *For any two $(M - d) \times Q$ matrices $\mathbf{Y}_1$ and $\mathbf{Y}_2$, if both matrices have rank L, and can be factorized as*

$$\mathbf{Y}_1 = \mathbf{CD}, \qquad \mathbf{Y}_2 = \mathbf{C\Phi}^d\mathbf{D}, \tag{6}$$

where $d \geq 1$, $\min\{M - d, Q\} \geq L$, $\mathbf{C}$ is an $(M - d) \times L$ matrix, $\mathbf{D}$ is an $L \times Q$ matrix, and $\mathbf{\Phi}$ (as well as $\mathbf{\Phi}^d$) is an $L \times L$ diagonal matrix with each diagonal element mapping to one of the desired parameters uniquely, then the desired parameters can be uniquely determined by the generalized eigenvalues of the matrix pencil $(\mathbf{Y}_1 - \xi\mathbf{Y}_2)$, for example, the desired parameters are the frequencies in the harmonic retrieval problem.

Proof. According to the property that the rank of the product of matrices is smaller than the rank of any factor matrix, both $\mathbf{C}$ and $\mathbf{D}$ have rank L.

For the pencil $(\mathbf{Y}_1 - \xi\mathbf{Y}_2) = \mathbf{C}(\mathbf{I} - \xi\mathbf{\Phi}^d)\mathbf{D}$, if ξ_ℓ is a generalized eigenvalue of the pencil, the matrix $\mathbf{C}(\mathbf{I} - \xi_\ell\mathbf{\Phi}^d)\mathbf{D}$ will have rank $L - 1$. This implicitly requires the matrix $\mathbf{I} - \xi_\ell\mathbf{\Phi}^d$ to be rank deficient [18, page 48]. Thus, ξ_ℓ equals the reciprocal of one of the diagonal elements of $\mathbf{\Phi}^d$, and the desired parameter can be determined accordingly. □

This theory removes the normal constraints on the structures of the basic factor matrices (e.g., Vandermande matrix) and the data matrices (e.g., Hankel or Toeplitz matrix). Any problem can be solved applying this theory if it can be formulated likewise. An example is if the parameters in $\mathbf{\Phi}$ are independent of those in $\mathbf{C}$ and $\mathbf{D}$, they can still be determined no matter how many unknown parameters are contained in $\mathbf{C}$ and $\mathbf{D}$.

3.2. Principal subspace and frequency estimation

Suppose that the formed $\mathbf{Y}_1$ and $\mathbf{Y}_2$ are $(M-d)\times Q$ noise-free matrices. Since $\mathbf{Y}_1$ has rank L, the compact SVD of $\mathbf{Y}_1$ has the form

$$\begin{aligned}\mathbf{Y}_1 &= \mathbf{U\Lambda V}^* \\ &= \begin{bmatrix}\mathbf{U}_p & \mathbf{U}_r\end{bmatrix}\begin{bmatrix}\mathbf{\Lambda}_p & \mathbf{0} \\ \mathbf{0} & \mathbf{\Lambda}_r\end{bmatrix}\begin{bmatrix}\mathbf{V}_p & \mathbf{V}_r\end{bmatrix}^* \\ &= \mathbf{U}_p\mathbf{\Lambda}_p\mathbf{V}_p^* + \mathbf{U}_r\mathbf{\Lambda}_r\mathbf{V}_r^*,\end{aligned} \tag{7}$$

where the $L \times L$ diagonal matrix $\mathbf{\Lambda}$ contains singular values in descending order, the $(M-d)\times L$ matrix $\mathbf{U}$ and $Q\times L$ matrix $\mathbf{V}$ consist of left and right singular vectors, respectively. $\mathbf{U}_p(\mathbf{V}_p)$ and $\mathbf{U}_r(\mathbf{V}_r)$ are the left and right submatrices of $\mathbf{U}(\mathbf{V})$, associated with the p principal and the remaining $r = L - p$ smaller singular values, respectively.

Multiplying the matrix pencil $(\mathbf{Y}_1 - \xi\mathbf{Y}_2)$ by $\mathbf{U}_p^*$ from the left and by $\mathbf{V}_p$ from the right, we get a new $p\times p$ matrix pencil

$$(\mathbf{\Lambda}_p - \xi\mathbf{U}_p^*\mathbf{Y}_2\mathbf{V}_p), \tag{8}$$

where we have utilized the orthogonality between the columns of $\mathbf{U}_p$ and $\mathbf{U}_r$, and $\mathbf{V}_p$ and $\mathbf{V}_r$.

For the new matrix pencil, we have the following results.

Proposition 2. *For the two $(M - d) \times Q$ matrices $\mathbf{Y}_1$ and $\mathbf{Y}_2$ defined in Proposition 1, when the generalized eigenvalues of the matrix pencil $(\mathbf{I} - \xi\mathbf{\Phi}^d)\mathbf{DV}_p$ exist, the matrix pencil $(\mathbf{\Lambda}_p - \xi\mathbf{U}_p^*\mathbf{Y}_2\mathbf{V}_p)$ has p distinct generalized eigenvalues ξ_ℓ, $\ell = 1, 2, \ldots, p$, and, specific to a harmonic retrieval problem, the angles of ξ_ℓ equal to the p frequencies ω_ℓ up to a known scalar, corresponding to p harmonics with largest energy.*

Proof. As defined in Proposition 1, $\mathbf{Y}_1$ and $\mathbf{Y}_2$ can be factorized as

$$\mathbf{Y}_1 = \mathbf{CD}, \qquad \mathbf{Y}_2 = \mathbf{C\Phi}^d\mathbf{D}, \tag{9}$$

where $\mathbf{C}$ is an $(M - d) \times L$ matrix with rank L, and $\mathbf{D}$ is an $L \times Q$ matrix with rank L.

Let $\mathbf{U}_L$ $(\mathbf{V}_L)$ denote the matrix containing L dominant left (right) singular vectors of $\mathbf{Y}_1$, and $\mathbf{\Lambda}_L$ the corresponding diagonal singular values matrix. According to

$$\begin{aligned}\text{Rank}(\mathbf{U}_L^*\mathbf{Y}_1) &= \text{Rank}(\mathbf{\Lambda}_L\mathbf{V}_L^*) = L \\ &= \text{Rank}(\mathbf{U}_L^*\mathbf{CD}) \leq \text{Rank}(\mathbf{U}_L^*\mathbf{C}),\end{aligned} \tag{10}$$

we know Rank $(\mathbf{U}_L^*\mathbf{C}) = L$, where we used the property that the rank of a product matrix could not be larger than the rank of every factor matrix.

Similarly, we can get Rank $(\mathbf{DV}_p) = p$.

Then for the matrix

$$\mathbf{U}_L^*(\mathbf{Y}_1 - \xi\mathbf{Y}_2)\mathbf{V}_p = \underbrace{\mathbf{U}_L^*\mathbf{C}}_{L\times L}\underbrace{(\mathbf{I} - \xi\boldsymbol{\Phi}^d)}_{L\times L}\underbrace{\mathbf{DV}_p}_{L\times p}, \tag{11}$$

if ξ is the generalized eigenvalue of the pencil $(\mathbf{I} - \xi\boldsymbol{\Phi}^d)\mathbf{DV}_p$ (we will discuss the possibility of its existence later), it is also a rank-reducing number of the matrix $(\mathbf{I} - \xi\boldsymbol{\Phi}^d)\mathbf{DV}_p$. This implies $(\mathbf{I} - \xi\boldsymbol{\Phi}^d)$ is rank deficient. Otherwise Rank$((\mathbf{I} - \xi\boldsymbol{\Phi}^d)\mathbf{DV}_p) = p$. Therefore ξ is also a rank reducing number of the matrix $(\mathbf{I} - \xi\boldsymbol{\Phi}^d)$ and the eigenvalue corresponding to ω_ℓ is

$$\xi_\ell = e^{-jd\omega_\ell}. \tag{12}$$

On the other hand, the generalized eigenvalue problem can be reduced to the standard eigenvalue problem [19] by

$$\xi(\mathbf{Y}_1, \mathbf{Y}_2) = \xi(\mathbf{Y}_2^\dagger\mathbf{Y}_1) = \xi^{-1}(\mathbf{Y}_1^\dagger\mathbf{Y}_2), \tag{13}$$

where the generalized eigenvalues ξ are expressed as functions of matrix pencil and matrix product, provided that the pseudoinverse matrices of $\mathbf{Y}_1$ and $\mathbf{Y}_2$ exist. Thus the generalized eigenvalue in (11) can be written as

$$\begin{aligned}\xi(\mathbf{U}_L^*\mathbf{Y}_1\mathbf{V}_p, \mathbf{U}_L^*\mathbf{Y}_2\mathbf{V}_p) &= \xi\left(\begin{bmatrix}\boldsymbol{\Lambda}_p\\ \mathbf{0}\end{bmatrix}, \mathbf{U}_L^*\mathbf{Y}_2\mathbf{V}_p\right)\\ &= \xi^{-1}\left(\begin{bmatrix}\boldsymbol{\Lambda}_p\\ \mathbf{0}\end{bmatrix}^\dagger \mathbf{U}_L^*\mathbf{Y}_2\mathbf{V}_p\right)\\ &= \xi^{-1}(\boldsymbol{\Lambda}_p^{-1}\mathbf{U}_p^*\mathbf{Y}_2\mathbf{V}_p)\\ &= \xi(\boldsymbol{\Lambda}_p, \mathbf{U}_p^*\mathbf{Y}_2\mathbf{V}_p).\end{aligned} \tag{14}$$

From (12) and (14), we have

$$\omega_\ell = \frac{\text{Phase}(\xi(\boldsymbol{\Lambda}_p, \mathbf{U}_p^*\mathbf{Y}_2\mathbf{V}_p))}{d}, \quad d \geq 1. \tag{15}$$

We have seen from above that both $\boldsymbol{\Lambda}_p$ and $\mathbf{U}_p^*\mathbf{Y}_2\mathbf{V}_p$ are full rank, so there are totally p generalized eigenvalues of the pencil $\boldsymbol{\Lambda}_p - \xi\mathbf{U}_p^*\mathbf{Y}_2\mathbf{V}_p$ [19, page 375], corresponding to p frequencies.

Since the SVD of a matrix exhibits the spectral distribution of the comprised signal in harmonic retrieval problems [11], the principal singular values and vectors reflect the information of the frequencies with largest power. This intuitively explains why the p generalized eigenvalues are associated with the p frequencies with largest energy. □

So far, we have established the links between the angles of the p generalized eigenvalues and the frequencies. However, an extra condition has to be emphasized in the above proof: whether those generalized eigenvalues of the pencil $(\mathbf{I} - \xi\boldsymbol{\Phi}^d)\mathbf{DV}_p$ exist or not? There may not exist a clear answer since in our experiments, it varies from time to time.

If the generalized eigenvalues of $(\mathbf{I} - \xi\boldsymbol{\Phi}^d)\mathbf{DV}_p$ *do not exist, the obtained eigenvalues* ξ *become good approximations to the actual ones when* p *is not very small compared to* L. Because in this case, the $p \times p$ pencil can be viewed as an approximation of the original one, or ξ can be regarded as the frequency estimates of the p harmonics with larger energy under the interference of the remaining $L - p$ harmonics with lower energy. To characterize the errors of this approximation, the general perturbation analysis [19] could be used. However, we note that it is not very suitable here because the elements in the perturbation matrix are not small enough.

3.3. Energy/amplitude estimation of the harmonics

In the case when only p out of L frequencies are known, the amplitude estimates obtained by solving the underdetermined linear equations of (1) will comprise large errors. Alternatively, when $\mathbf{Y}_1$ and $\mathbf{Y}_2$ are formed as the correlation matrices of $x(k)$, for example,

$$\mathbf{Y}_1 = \mathbf{X}_{\downarrow d}(\mathbf{X}_{\downarrow d})^*, \qquad \mathbf{Y}_2 = \mathbf{X}^{\uparrow d}(\mathbf{X}_{\downarrow d})^*, \tag{16}$$

the energy of the harmonics can be estimated in a subspace method according to the following proposition.

Proposition 3. *When* $\mathbf{Y}_1$ *and* $\mathbf{Y}_2$ *are constructed in the way similar to* (16)*, the energy of* ℓ*th harmonic,* $|a_\ell|^2$*, can be well approximated as*

$$|a_\ell|^2 = \frac{\boldsymbol{\theta}_\ell^*\boldsymbol{\Lambda}_p\boldsymbol{\theta}_\ell}{|\boldsymbol{\theta}_\ell^*\mathbf{U}_p^*\mathbf{f}(M-d;\omega_\ell)|^2}, \tag{17}$$

where $\boldsymbol{\theta}_\ell$ *is the generalized eigenvector corresponding to the generalized eigenvalue* ξ_ℓ *(and then frequency* ω_ℓ*), and* $\mathbf{f}(M - d;\omega_\ell)$ *is defined in* (4).

Proof. See the appendix. □

From the proof, we can see that a necessary condition for the above proposition is that the product $\mathbf{F}_Q^T(\mathbf{F}_Q^T)^*/Q$ needs to resemble an identity matrix. Actually, the (ℓ_1, ℓ_2)th element of $\mathbf{F}_Q^T(\mathbf{F}_Q^T)^*$ is given by

$$\begin{aligned}\mathbf{f}(Q;\omega_{\ell_1})^T(\mathbf{f}(Q;\omega_{\ell_2})^T)^* &= \sum_{q=1}^{Q} e^{jq(\omega_{\ell_1}-\omega_{\ell_2})}\\ &= \frac{e^{j(\omega_{\ell_1}-\omega_{\ell_2})} - e^{j(Q+1)(\omega_{\ell_1}-\omega_{\ell_2})}}{1 - e^{j(\omega_{\ell_1}-\omega_{\ell_2})}}.\end{aligned} \tag{18}$$

Figure 1 demonstrates the magnitude of these elements. From the figure, it is obvious that, only when Q is large enough and there is no frequency close to zero or 2π, can $\mathbf{F}_Q^T(\mathbf{F}_Q^T)^*/Q$ be approximated as an identity matrix and the above method works. In practical applications, when this condition is not satisfied, we need to consider alternative approaches.

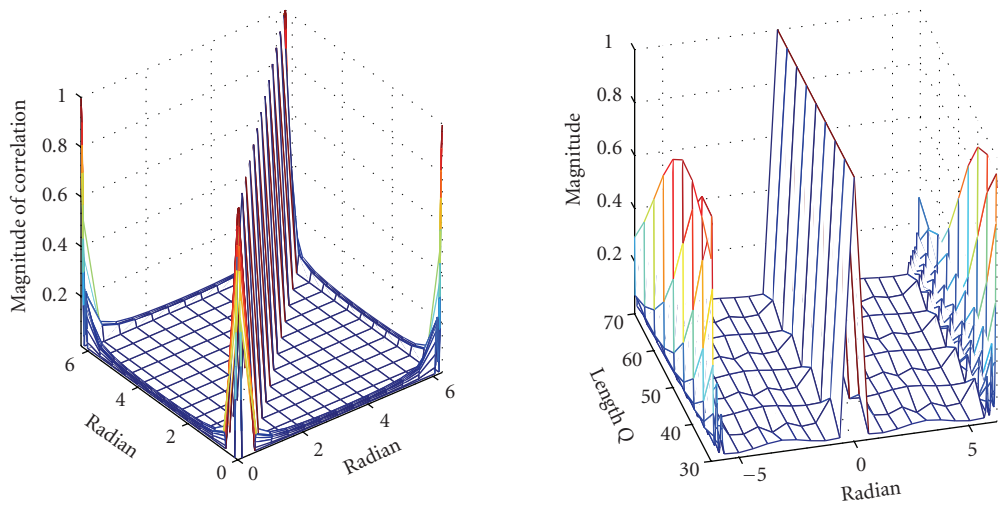

(a) Correlation (b) Element of matrix

FIGURE 1: Illustration of the entries of $\mathbf{F}_Q^T(\mathbf{F}_Q^T)^*$: (a) magnitude of correlation coefficients for a fixed $Q = 50$; (b) magnitude of the elements in (18) versus various Q and the difference $\omega_{\ell_1} - \omega_{\ell_2}$.

The two key factors in the derivation of (17) are that (1) $\mathbf{Y}_1$ is symmetric and (2) a_ℓ, $\ell \in [1, L]$ is fully contained in a diagonal matrix, and each of them can be mapped to one of the diagonal elements uniquely. These observations motivate us to construct the following $M \times Q$ data matrices

$$\begin{aligned}\mathbf{Y}_1 &= \begin{pmatrix} x(0) & x(-1) & \cdots & x(1-Q) \\ x(1) & x(0) & \cdots & x(2-Q) \\ \vdots & \vdots & \ddots & \vdots \\ x(M-1) & x(M-2) & \cdots & x(M-Q) \end{pmatrix} \\ &= \mathbf{F}_M \mathbf{A} \mathbf{F}_Q^*, \\ \mathbf{Y}_2 &= \begin{pmatrix} x(d) & \cdots & x(d+1-Q) \\ x(d+1) & \cdots & x(d+2-Q) \\ \vdots & \ddots & \vdots \\ x(M-1+d) & \cdots & x(M-Q+d) \end{pmatrix} \\ &= \mathbf{F}_M \mathbf{\Phi}^d \mathbf{A} \mathbf{F}_Q^*, \end{aligned} \tag{19}$$

where $\min\{M, Q\} \geq L$ and $d \geq 1$.

These two matrices have the shift-invariant property, and the diagonal elements of $\mathbf{\Phi}$ can be determined by the generalized eigenvalues of the matrix pencil $(\mathbf{Y}_1 - \xi \mathbf{Y}_2)$. The reduced rank algorithms described in Proposition 2 are also applicable to this pencil. Now, if we let $M = Q$, and assume $\mathbf{A}$ is a real matrix (a_ℓ are real), $\mathbf{Y}_1$ will be a Hermitian matrix. For a Hermitian but not necessarily positive-definite matrix, the eigenvalues are real but not necessarily positive. Therefore, to maintain its singular values positive, the left and right singular vectors of the matrix are equal up to a constant diagonal matrix $\hat{\mathbf{I}}$. This matrix $\hat{\mathbf{I}}$ has diagonal entries -1 or 1 corresponding to the polarity of the eigenvalues. For example, $\mathbf{U}_p = \mathbf{V}_p \hat{\mathbf{I}}_p$ for the p principal singular vectors.

Then, similar to the proof of Proposition 3, the following proposition can be proven. Note that the matrices $\mathbf{P}$ in (A.1) in the proof of Proposition 3 will be replaced by $\mathbf{A}$. This change leads to the estimates of amplitudes rather than squared amplitudes.

Proposition 4. *When $\mathbf{Y}_1$ and $\mathbf{Y}_2$ are constructed in the way similar to (19) with $M = Q$, and $\mathbf{A}$ is a real diagonal matrix with diagonal entries equal to the amplitudes of harmonics, the amplitude of ℓth harmonic, a_ℓ, can be determined by*

$$a_\ell = \frac{\boldsymbol{\theta}_\ell^* \hat{\mathbf{I}}_p \mathbf{\Lambda}_p \boldsymbol{\theta}_\ell}{\left| \boldsymbol{\theta}_\ell^* \hat{\mathbf{I}}_p \mathbf{U}_p^* \mathbf{f}(M; \omega_\ell) \right|^2}, \tag{20}$$

where $\boldsymbol{\theta}_\ell$ is the generalized eigenvector corresponding to the generalized eigenvalue ξ_ℓ (and then frequency ω_ℓ).

It is obvious that this result is superior to the one in Proposition 3 in the estimation of a_ℓ. However, there is another problem associated with it. Since $\mathbf{Y}_1$ is a Hermitian matrix directly constructed from the samples, the performance of the frequency estimation might be inferior to the one in Proposition 3 when the dimensions of these two matrices are equal. This happens when the added noise matrix is also Hermitian, because in this case, the number of effective samples in Proposition 4 equivalently reduces to half. Even so, it might still be worthy of constructing a double size matrix and using our RIPC algorithms when fast algorithms can largely reduce the cost of computation, compared to the general L-rank algorithms. This is confirmed by some experimental results to be given in Section 5.

3.4. Fast algorithms to find the principal signal space

Since only p out of L principal singular values and vectors are required, the computation can be simplified by applying fast

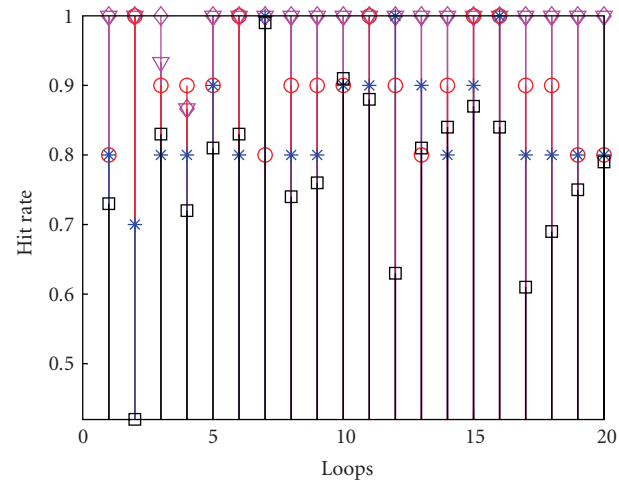

(a) Hit rate of the frequency estimates

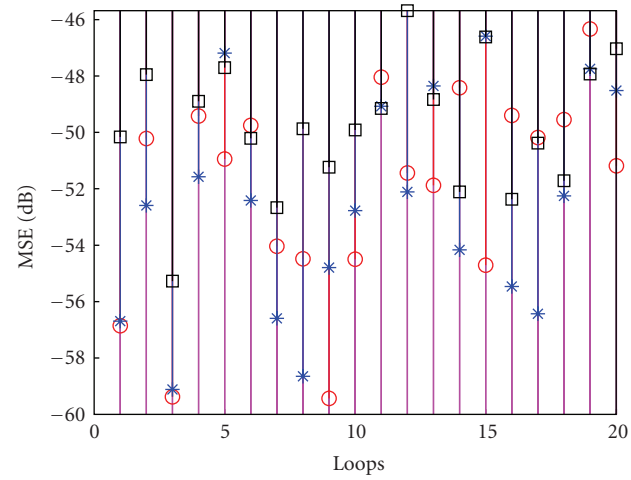

(b) MSE of the frequency estimates

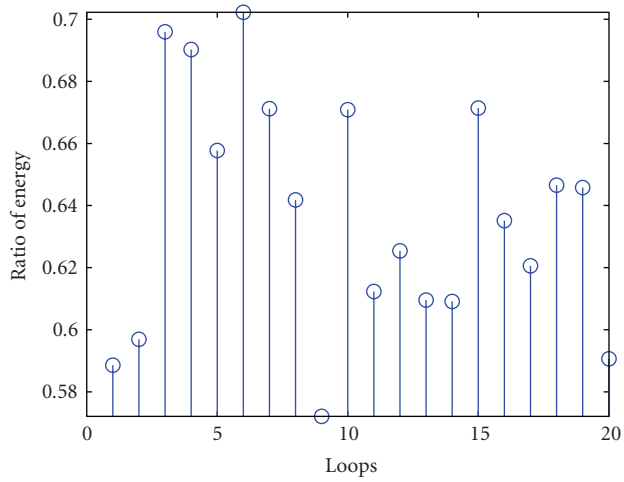

(c) The ratio of collected energy

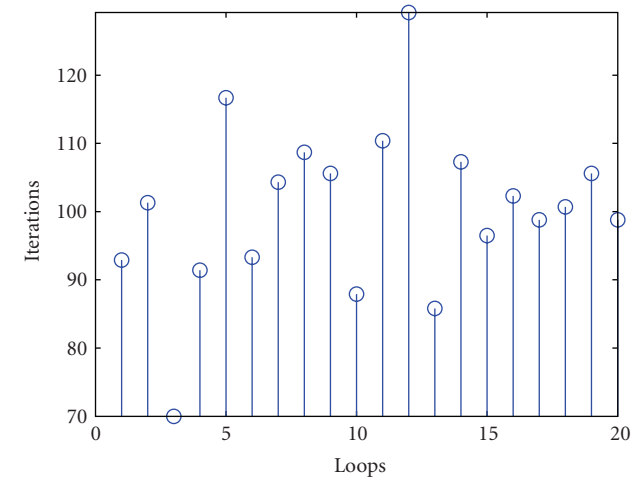

(d) Iterations in the power method

FIGURE 2: Implementations of A1–A5 in the noise-free case with $p = 10$, $L = 50$, and $M = 60$. Stems marked with diagonals, downward triangles, circles, stars, and squares denote the algorithms A1–A5, respectively. These legends also apply to Figure 3.

algorithms with lower complexity, such as the power method [19]. For each dominant singular value and vector, the power method has a computational order of M^2 for an $M \times M$ Hermitian matrix. To be stated, in the power method, the speed of convergence depends on the ratio between the two largest singular values of the matrix. The larger the ratio is, the faster it converges.

For an $M \times M$ Hermitian matrix $\mathbf{Y}_1$, the power method generates p principal singular values and vectors as shown in Algorithm 1.

When $\mathbf{Y}_1$ is not a Hermitian matrix, a similar algorithm is applicable in which the left and right singular vectors should be generated by constructing $\mathbf{Y}_1\mathbf{Y}_1^*$ and $\mathbf{Y}_1^*\mathbf{Y}_1$, respectively.

On the detailed implementation of the power method, we have some interesting findings in our experiments.

(i) After the ith eigenvector is generated, if we let it be the initial iterative vector $\mathbf{q}^{(0)}$ in solving the next eigenvalue and vector rather than randomly chosen $\mathbf{q}^{(0)}$, the iteration usually converges very fast. For positive Hermitian matrices, 2 or 3 iterations are enough.

(ii) Even when the first several estimated eigenvalues contain larger errors, the remaining eigenvalues can still be estimated with higher accuracy due to the stability of eigenvalues to the perturbation errors.

(iii) If not all eigenvalues are positive, the power method might output eigenvalues in a nonordered manner. This usually implies relatively larger errors in these eigenvalues. However, the estimated frequencies can still have good accuracy.

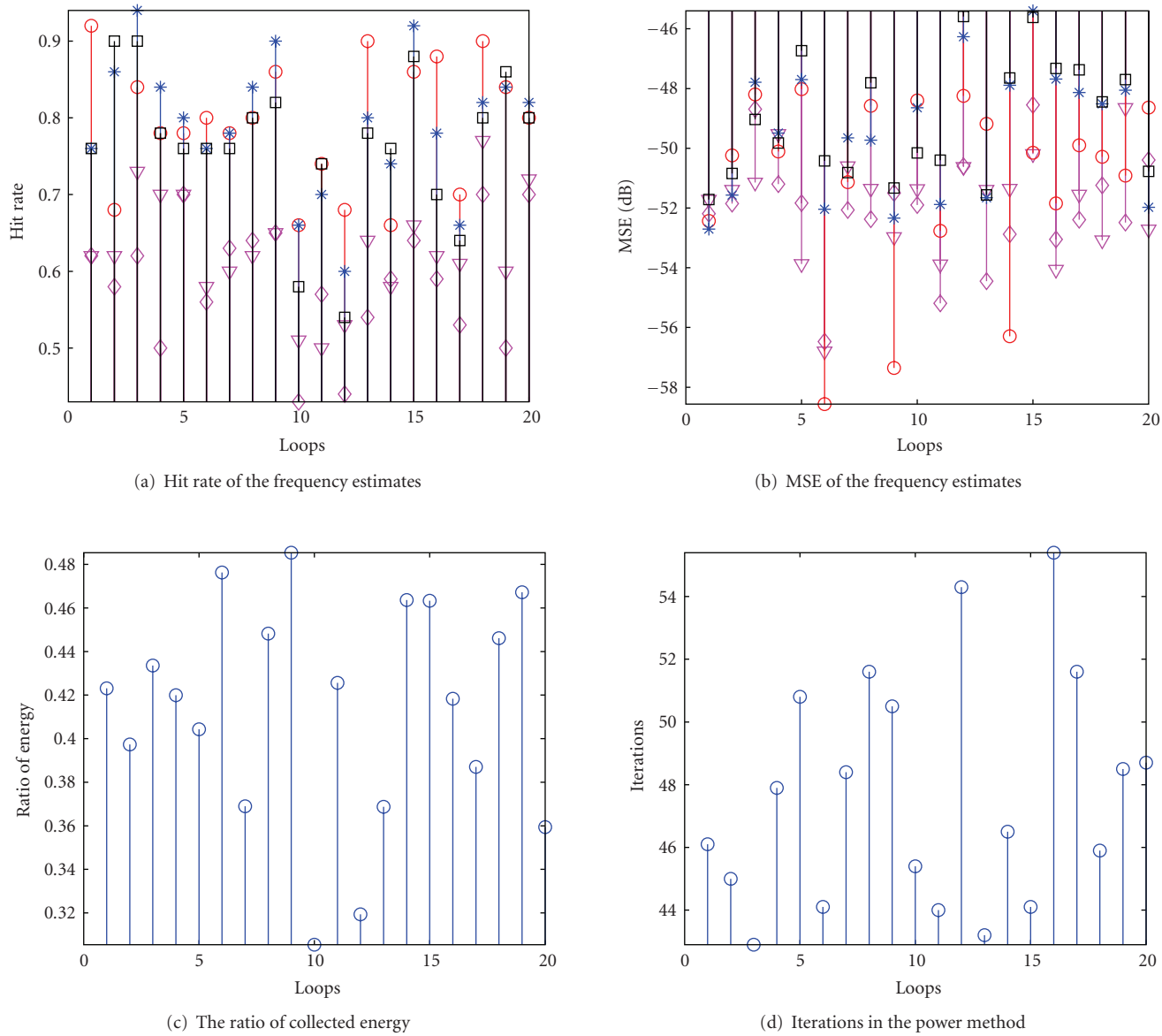

(a) Hit rate of the frequency estimates

(b) MSE of the frequency estimates

(c) The ratio of collected energy

(d) Iterations in the power method

FIGURE 3: Implementations of A1–A5 with $p = 5$, $L = 50$, SNR = 5 dB, and $M = 60$.

It should be noted that although the generalized eigenvalues of the pencil $(\mathbf{Y}_1 - \xi\mathbf{Y}_2)$ are equal to the eigenvalues of $(\mathbf{Y}_2^{\dagger}\mathbf{Y}_1)$, the power method is ineffective in directly solving the first p eigenvalues of $(\mathbf{Y}_2^{\dagger}\mathbf{Y}_1)$ because there are not large enough gaps between adjacent eigenvalues (the magnitudes of all eigenvalues equal 1).

4. JOINT SYNCHRONIZATION AND CHANNEL IDENTIFICATION

We consider a general transmitted UWB signal $s(t)$ in a single-user system. The signal $s(t)$ could be a spread spectrum (SS) signal (e.g., time-hopping or direct sequence spread) or non-SS signal (e.g., single pulse), but it should be unmodulated or modulated with known constant data. For randomly modulated signals, the sampled channel impulse response can be estimated using the least squares criterion first as discussed in [4]. We assume that the spread spectrum codes are known in an SS system.

Here, the used UWB multipath channel model is a simplified version of the IEEE802.15.3a channel model [15], which is a modified Saleh-Valenzuela model where multipath components arrive in clusters. For synchronization and channel estimation, the IEEE model can be simplified to a TDL model, represented by

$$h(t) = \sum_{\ell=1}^{L} a_\ell \delta(t - \tau_\ell), \tag{21}$$

where τ_ℓ is the ℓth multipath delay, a_ℓ is the ℓth multipath gain with phase randomly set to $\{\pm 1\}$ with equal probability, L is the number of multipaths, and $\delta(\cdot)$ is the Dirac delta

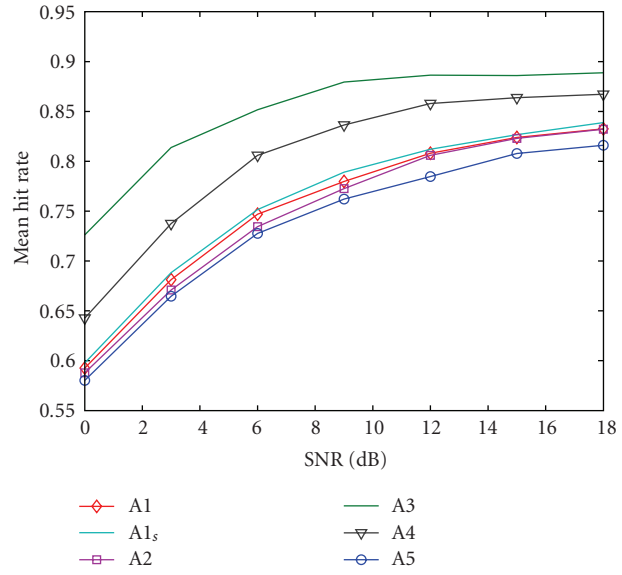

(a) Mean hit rate of the frequency estimates

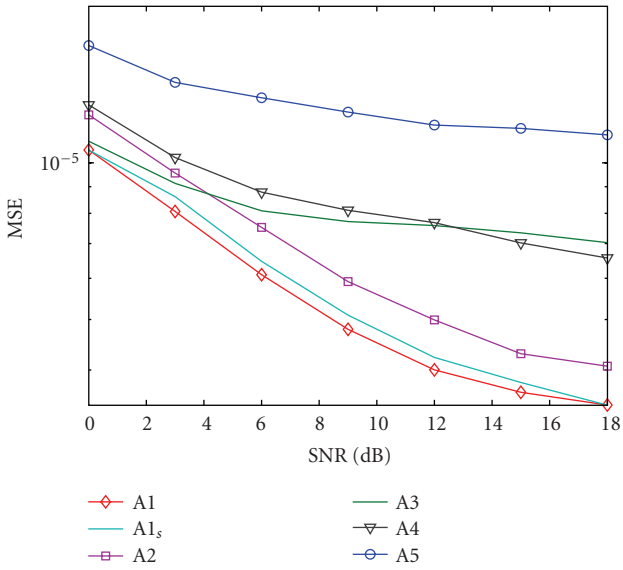

(b) Averaged MSE of the frequency estimates

FIGURE 4: The averaged hit rate (a) and MSE (b) versus the SNR in the algorithms A1–A5 when $p = 10$, $L = 50$, and $M = 60$ for A1, A1$_s$, A3, $M = 120$ for others.

function. The multipath delay τ_ℓ and gain a_ℓ are regarded as deterministic parameters to be estimated.

When a symbol sequence $\{s_i(t)\}$ is transmitted over this channel, the received signal $r(t)$ is

$$r(t) = \sum_i \sum_{\ell=1}^{L} a_\ell s_i(t - iT_s - \tau - \tau_\ell) + n(t), \qquad (22)$$

where $n(t)$ is the additive white Gaussian noise (AWGN), τ is the synchronization delay between the receiver and the transmitter, and T_s is the symbol period.

To set up the connection between (22) and (1), we can transform (22) from time domain to frequency domain by applying the Discrete Fourier Transform (DFT) upon the samples of $r(t)$.

(1) Let $i = 1$, and set the desired number of iterations to J in the calculation of every singular value and vector(Note: Besides this pre-defined J, a threshold can also be set to jump out the iterations once the squared error between two latest generated eigenvalues is smaller than this threshold.);

(2) Generate the dominant real eigenvalue $\lambda_i = \lambda_i^{(J)}$ and left eigenvector $\mathbf{u}_i = \mathbf{u}_i^{(J)}$ of $\mathbf{Y}_1$ using the power method described below: Generate a unit 2-norm vector $\mathbf{q}^{(0)} \in \mathbb{C}^M$ randomly;

for $j = 1, 2, \ldots, J$

$$\mathbf{u}_i^{(j)} = \mathbf{Y}_1 \mathbf{q}^{(j-1)}$$
$$\mathbf{q}^{(j)} = \mathbf{u}_i^{(j)} / \|\mathbf{u}_i^{(j)}\|_2$$
$$\lambda_i^{(j)} = [\mathbf{q}^{(j)}]^* \mathbf{Y}_1 \mathbf{q}^{(j)}$$

end

where $\|\cdot\|_2$ is the vector 2-norm;

(3) If $\lambda_i < 0$, let $\lambda_i = -\lambda_i$, and the right eigenvector $\mathbf{v}_i$ be $\mathbf{v}_i = -\mathbf{u}_i$; Otherwise, let $\mathbf{v}_i = \mathbf{u}_i$;

(4) Use the *deflation* operation to update $\mathbf{Y}_1$:

$$\mathbf{Y}_1 = \mathbf{Y}_1 - \lambda_i \mathbf{u}_i \mathbf{v}_i^*;$$

(5) Let $i = i + 1$, and repeat 2 until $i = p + 1$.

ALGORITHM 1: Algorithm to generate p principal singular values and vectors of a $M \times M$ Hermitian matrix $\mathbf{Y}_1$ using the power method.

4.1. Sampling of signals

Since the system is not synchronized yet, whatever the signal $s(t)$ is, the width of the sampling window should be chosen to equal the integral multiple of the symbol period and be larger than the maximal multipath spread T_m. Assume that the sampling period is T, the number of samples is K_1, and the samples from (22) are $\{r(m)\}$, $m \in [0, K_1 - 1]$. Two scenarios regarding to the sampling need to be considered.

(1) Sampling of widely separated pulses

When the intervals between the continuously transmitted pulses are larger than T_m, there is no ISI in the samples. Let the sampling length TK_1 equal the symbol period T_s, $\{s(m)\}$ be the samples of $s_i(t)$, and $\{n(m)\}$ be the samples of the noise $n(t)$, then the DFT coefficients of (22) can be represented as

$$R(k) = S(k) \sum_{\ell=1}^{L} a_\ell e^{-jk\Omega_0(\tau+\tau_\ell)} + N(k), \quad k \in [0, K_1 - 1], \qquad (23)$$

where $\Omega_0 = 2\pi/(TK_1)$ is the basic frequency, $S(k)$ and $N(k)$ are the DFT coefficients of $\{s(m)\}$ and $\{n(m)\}$, respectively.

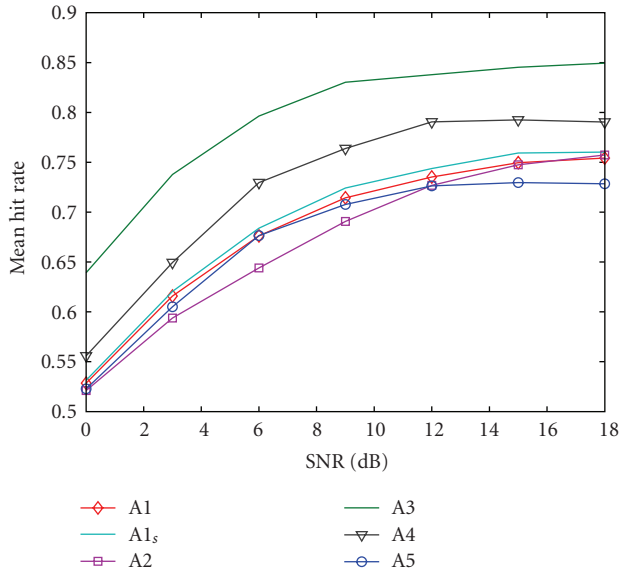

(a) Mean hit rate of the delay estimates

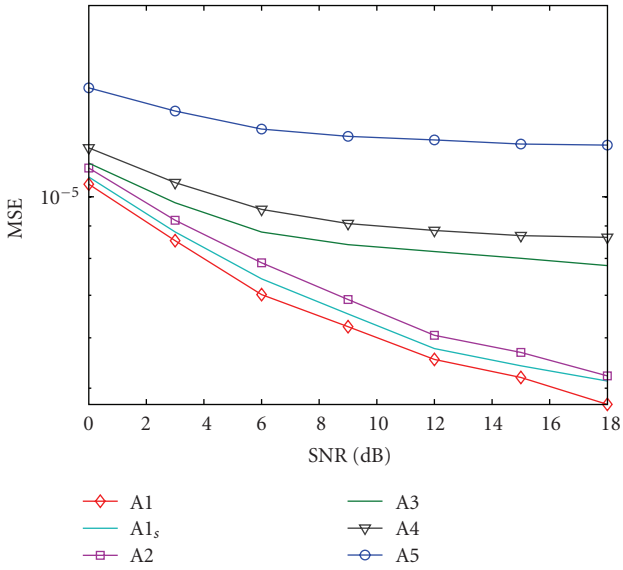

(b) MSE of the delay estimates

FIGURE 5: The averaged hit rate (a) and MSE (b) versus the SNR in the algorithms A1–A5 when $p = 10$, $L = 50$, and $M = 60$ for A1, A1$_s$, A3, $M = 120$ for others. The parameters of harmonics are from the IEEE channel model.

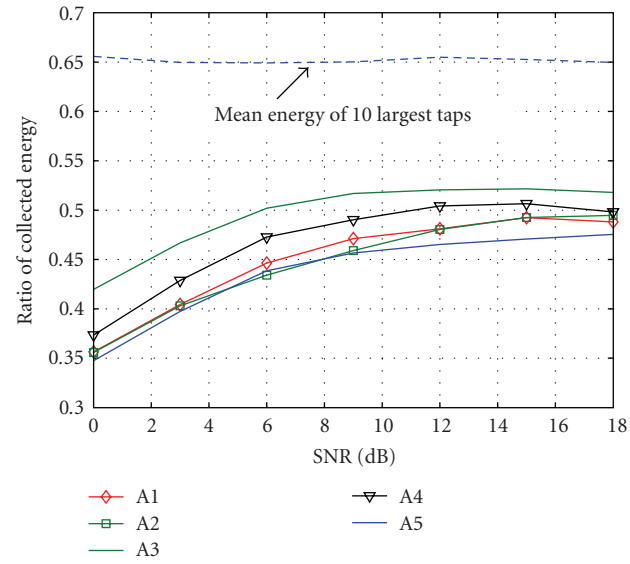

FIGURE 6: The mean ratio of the collected energy by A1–A5, corresponding to the results in Figure 5.

(2) Sampling of closely spaced pulses

When the intervals between the transmitted pulses are smaller than T_m, ISI is generated. Assume that the multipath can be fully covered by at most Δi symbols, that is, $T_s \Delta i \geq T_m$. Represent the Δi symbols as

$$s_{\Delta i}(t) = \sum_{i=i_1}^{i_1+\Delta i-1} s_i(t - iT_s), \tag{24}$$

where i_1 is the index of any symbol, and let $\{s(m)\}$, $m \in [1, K_1]$ be the samples of $s_{\Delta i}(t)$. In this case, the samples of $r(t)$, $\{r(m)\}$, contain ISI terms. However, when symbols are transmitted continuously without interruption, it can be proven that $R(k)$, the DFT coefficients of $\{r(m)\}$, are ISI-free due to the *Circular Shift Property* [20, page 536] of DFT, and (23) also holds.

This finding enables continuous transmission of the training sequence to speed the synchronization process. This is also another advantage of the proposed algorithms compared to conventional algorithms which generally require the interval between two impulses to be larger than the multipath delay spread.

4.2. *Summary of joint synchronization and channel identification schemes using RIPC algorithms*

Deconvolution is defined as the operation of dividing $R(k)$ by $S(k)$ in (23), the reverse of convolution viewed in the frequency domain. After the deconvolution operation, we get some equations identical to (1) in the harmonic retrieval problem. Then the synchronization and channel identification algorithm can be summarized as follows:

(1) in a window with width TK_1, sample the received signal with period T. Make sure TK_1 equals an integral multiple of the symbol period T_s and larger than the multipath spread T_m;

(2) apply the FFT to the samples and select K DFT coefficients carefully;

(3) after deconvolution, form the Hankel data matrix $\mathbf{X}$, and use principal components tracking algorithms to estimate the p delays with largest energy (sum of τ and τ_ℓ). (If the amplitudes a_ℓ are required, correlation matrices or Hermitian data matrices should be used.)

(4) resolve τ and τ_ℓ from the estimated delays.

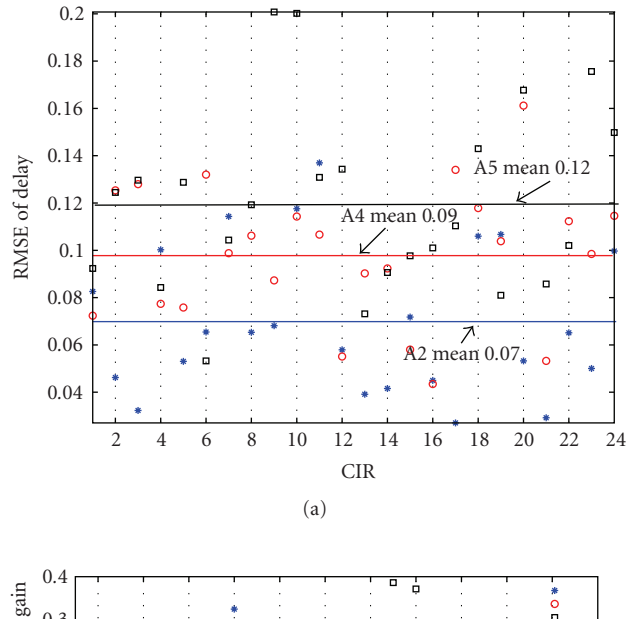

Figure 7: Performance of estimates in the noise-free case when $T = 0.3t_p$, $p = 10$, $L = 50$, and $M = 60$. From top to bottom: normalized RMSEs of the delay estimates, mean errors of the gain estimates and hit rates of the delay estimates. The horizontal axis in each subplot represents CIR realizations.

The last step is necessary as each estimated delay in step (3) is the sum of the synchronization delay τ and one of the multipath delays τ_ℓ. There is a phase-ambiguity problem with these sums as the delays may become circularly shifted. This could happen when sampling starts in the middle of multipath delays. Our solution is first to choose TK_1 much larger than the maximal multipath delay T_m, then separate τ and τ_ℓ according to the following criteria.

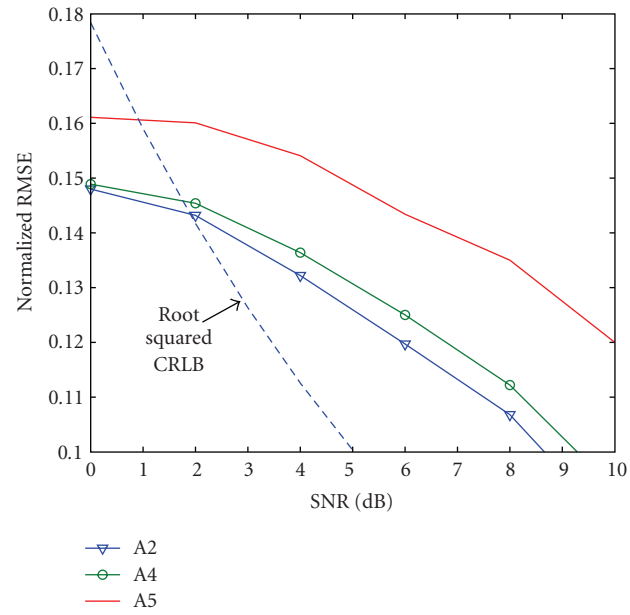

Figure 8: Normalized RMSE of the delay estimates versus the SNR where $T = 0.3t_p$, $p = 10$, $L = 50$, and $M = 60$.

(i) Sort the estimates in ascending order and get $\{\hat{\tau}_1, \hat{\tau}_2, \ldots, \hat{\tau}_p\}$. If the gap between any two adjoining estimates is larger than a threshold τ_{th}, for example, $\hat{\tau}_{p_1} - \hat{\tau}_{p_1-1} > \tau_{\text{th}}$, then $\hat{\tau}_{p_1}$ equals the sum of the synchronization delay τ and the first desired multipath delay. And all the estimates need to be updated to

$$\{\hat{\tau}_{p_1}, \hat{\tau}_{p_1+1}, \ldots, \hat{\tau}_p, \hat{\tau}_1 + TK_1, \ldots, \hat{\tau}_{p_1-1} + TK_1\}, \tag{25}$$

that is, the original $\hat{\tau}_1, \ldots, \hat{\tau}_{p_1-1}$ are updated by adding TK_1 to themselves. Now, the receiver can synchronize to the multipath with delay $\hat{\tau}_{p_1}$ which implicitly assumes the delay of the first multipath of interest is zero, and the differences between the updated estimates and the first desired multipath are the relative multipath delays.

(ii) Otherwise, the smallest estimate is the first multipath of interest and no update is needed.

This judgement is based on the assumption that the gap between any two multipath signals is smaller than the threshold τ_{th}, which is generally close to the difference between the sampling window width TK_1 and the maximal multipath delay T_m. In practice, the multipath components with larger energy usually have smaller delays, so the threshold τ_{th} needs not be very large.

4.3. Complexity of our schemes

The complexity of our algorithms depends on the required resolution ability and performance of estimation. The resolution ability is roughly determined by the sampling

period. The smaller the sampling period is, the higher the resolution ability is. The performance of estimation is mainly influenced by the SNR, and the dimension of the matrices $\mathbf{Y}_1$ and $\mathbf{Y}_2$. Then the sampling period is the key parameter in both the complexity and performance since the main computation cost of our algorithm is associated with FFT, SVD, and GED. For a K_1-point FFT, the computational workload is $K_1(3\log_2 K_1 - 1)/2$ when a Cooley-Tukey radix-2 algorithm [21] is used. K_1 equals a power of 2. The complexity of GED for a $p \times p$ matrix is p^3. Plus the complexity of the power method (suppose that $K = K_1/2$ DFT coefficients are used), the total complexity is in the order of $K_1\log_2 K_1 + pK_1^2/4 + p^3$. Accordingly, the complexity of the general L-rank algorithms is in the order of $K_1\log_2 K_1 + K_1^3/8 + L^3$. When $L \gg p$, the saving is considerable.

5. SIMULATIONS

First, we show some experimental results of the RIPC algorithms using the harmonic retrieval model. The performance can act as a basis for evaluating the performance loss in many applications of RIPC algorithms. Simulation results of the joint synchronization and channel identification for UWB signals are given in Section 5.2.

5.1. Simulations of RIPC algorithms

The simulations in this subsection are based on the harmonic retrieval model in (1). The algorithms evaluated are classified as follows.

(A1) Algorithms A1 are full L-rank algorithms with a general matrix $\mathbf{Y}_1$ (not Hermitian nor positive-definite), where amplitudes are obtained by solving a Vandermonde problem using the least squares criterion.

(A2) Algorithms A2 are full L-rank algorithms with a Hermitian matrix $\mathbf{Y}_1$ (not positive-definite), where amplitudes can be estimated via (20) or by solving a Vandermonde matrix.

(A3) Algorithms A3 are RIPC algorithms with a general matrix $\mathbf{Y}_1$, where amplitudes cannot be estimated.

(A4) Algorithms A4 are RIPC algorithms with a Hermitian matrix $\mathbf{Y}_1$, where amplitudes are estimated by (20).

(A5) Algorithms A5 are RIPC algorithms with a Hermitian matrix $\mathbf{Y}_1$, where the power method is applied and amplitudes are estimated by (20).

We first generate amplitudes a_ℓ randomly using a Gaussian distribution with mean zero and variance 1. These amplitudes are normalized such that their squared sum is unity. The frequencies are generated randomly using a uniform distribution on the interval $[0, 2\pi)$. In most cases, $L = 50$ harmonics are generated, and 60×60 matrices $\mathbf{Y}_1$ and $\mathbf{Y}_2$ are constructed.

Figures 2 and 3 demonstrate some detailed implementations of algorithms A1–A5. Each figure consists of 4 subfigures. Figures 2(a) and 3(a) shows the *hit rate* of the frequency estimates. When an estimate has an estimation error within a predefined threshold (named as "hitting threshold" hereafter, set to 0.01), we say it "hits" the true value. The hit rate is then defined as the ratio between the number of the hit estimates and the total estimates. The hit rate is thus conceptually similar to the *outage probability* that is commonly used in the literature. Figures 2(b) and 3(b) shows the mean squared error (MSE) of the hit estimates (nonhit estimates are excluded) averaged over 10 realizations. The results obtained by algorithms A1–A5 are denoted by diagonals, triangles (down), circles, stars, and squares, respectively. Figures 2(c) and 3(c) shows the energy ratio of the p principal harmonics out of the total ones. Figures 2(d) and 3(d) shows the averaged number of iterations in the power method. In the power method, the maximal number of iterations in computing every eigenvalue and vector (J in Algorithm 1) is set to 30, and the threshold is set to 0.004 to control the number of iterations.

In Figure 2, simulation results in the noise-free case are illustrated with $p = 10$ and $L = 50$. It is clear that full L-rank algorithms A1 and A2 can achieve perfect estimation with high hit accuracy and near zero MSEs (not plotted in Figure 2(b)). Comparatively, our reduced-rank RIPC algorithms can not achieve perfect estimation in the noise-free case, while they are relatively stable with respect to the change of SNR.

Even when the samples are corrupted by noise, the algorithms A1 and A2 can normally achieve good frequency estimates for some harmonics, as can be observed in Figures 2 and 3. However, their amplitude estimates usually contain relatively larger error due to the following two reasons. On the one hand, the frequency estimates with higher accuracy normally correspond to the harmonics with larger energy according to the Cramer-Rao bound. For frequencies with smaller energy, the estimates inevitably contain larger errors. On the other hand, the accuracy of frequency estimates is due to the inherent stability of eigenvalues and singular values. The amplitude estimates, however, are susceptible to the noise. Thus, in the sense of determining p principal frequencies with largest energy, A1 is less effective than RIPC algorithms.

The ratio of collected energy shown in Figures 2 and 3(b) indicates that the hit rate and MSE are actually weakly dependent of the collected harmonics energy. This implies that an analytical analysis using an approximation theory (or the perturbation theory) for Proposition 2 might not work. Simultaneously, it implies that the stability of the RIPC algorithms is high with respect to the number p of the desired principal signals.

Figure 4 demonstrates how the hit rate and MSE vary with SNR where A1_s is a state space based algorithm within the framework of A1 used in [3]. From the figure, we see that when the SNR is larger (than 5 dB), the performance of the RIPC algorithms are satisfactory and stable.

In experiments, we find that the amplitude estimates in the RIPC algorithms are not so accurate as the frequency estimates because the errors in the frequency estimates are actually transferred into the amplitude estimates. In most cases, the polarity of the amplitude can be determined

accurately, while the magnitude can suffer an error as large as 30% of the true value in the SNR range 5–15 dB. This is a general problem in the subspace-based harmonic retrieval algorithms, which could be mitigated by averaging over multiple realizations. However, this problem does not influence the determination of p principal harmonics in RIPC algorithms as they have been automatically tracked and picked out during the frequency estimation.

5.2. Simulations of joint synchronization and channel identification

The second-order Gaussian monocycle $p(t)$ is used as the basic pulse

$$p(t) = \left[1 - 4\pi\left(\frac{t - t_p}{t_p}\right)^2\right] e^{-2\pi((t-t_p)/t_p)^2}, \qquad (26)$$

where t_p parameterizes the effective pulse width. The -3 dB bandwidth of this pulse is about $0.65/t_p$ Hz, -10 dB bandwidth is about $1.15/t_p$ Hz, and center frequency is about $0.8/t_p$ Hz.

When sampling this pulse with period $T = 0.3t_p$, we get roughly six samples per pulse, and this sampling rate is already above the Nyquist rate in terms of the -10 dB bandwidth. To reduce the sampling rate without introducing aliasing, similar to [3], a low-pass filter with bandwidth much smaller than the signal bandwidth can be applied at the cost of reduced energy collection. When choosing "clean" DFT coefficients to minimize interference due to residual alias, coefficients near the normalized frequency 0.5 should be excluded. On the other hand, DFT coefficients with larger energy should be chosen to avoid blowing up the noise in the *deconvolution* operation. When strong narrowband interference is present and the interference spectrum is known, the interference can be readily removed by selecting those coefficients in the unaffected spectrum.

To test the performance of our algorithms in practical implementations, we use the channel model CM1 proposed in [15] by IEEE802.15.3a. The channel impulse response (CIR) is reproduced using $t_p = 10^{-9}$. The first $L = 50$ multipath signals in each CIR are used to simulate the channel.

Before the actual implementations of synchronization and channel estimation, we first feed these multipath parameters into the harmonic retrieval model, that is, substitute a_ℓ with the multipath gains and ω_ℓ with $2\pi\tau_\ell/TK_1$ in (1), where TK_1 is chosen to be slightly larger than the maximal multipath delay T_m. The achievable performance can serve as upper bounds in practical implementations.

Figure 5 shows the hit rate and MSE of the frequency estimates in this case, and the actual collected energy by these algorithms is shown in Figure 6. To make the estimates independent of TK_1, estimates are kept in the form of frequencies rather than delays. It can be seen that there is not much difference between the performance here and that shown in Figure 4. This indicates the stability of our RIPC algorithms. From Figure 6, we can also see that about 80% energy of the 10 largest channel taps can be collected (and exploited then), which is consistent with the hit rate.

To check the performance loss in practical implementations, let us examine the noise-free case first. In the noise-free experiments, DFT coefficients from 0 to $0.4K_1$ are chosen, the hitting threshold is set to $0.25t_p$, and the estimates are compared with 15 principal multipath signals to determine the hits. Figure 7 shows the hit rate, root MSE (RMSE) of the delay estimates and mean error of the gain estimates obtained by A2, A4, and A5 with $p = 10$, $L = 50$, and $M = 60$. The RMSEs of the delay estimates are normalized with respect to t_p. The sampling rate is $0.3t_p$. In Figure 8, we show the RMSEs of the delay estimates versus the SNR for A2, A4, and A5. For comparison, the Cramer-Rao low bound (CRLB) in an AWGN channel [16] is also plotted. From the figures, we can see that an accuracy of about 10% of T_p can be obtained at average hit rate above 80%. This means that the timing accuracy is mostly within one sample distance, which is only slightly inferior to the full-rank approach in [3]. When the SNR is as large as 10 dB, the RMSEs are already very close to those in the noise-free case. Overlapping of the CRLB curve with other performance curves is due to the lower hit rate at smaller SNRs, where quite a few estimates with larger errors are excluded from the computation of the MSE. With the hit rate increasing, the CRLB curve becomes a good reference for evaluating the performance of the proposed schemes.

6. CONCLUSIONS

To reduce the complexity of general subspace-based delay estimation algorithms, we proposed reduced-rank shift-invariant techniques which can track the principal components automatically. Amplitude estimation schemes are also proposed based on subspace methods. Application of the proposed techniques in synchronization and channel estimation for UWB signals is investigated. Experiments show that our proposed algorithms can achieve performance comparable to full-rank algorithms, but with significantly reduced complexity.

APPENDIX

Proof of Proposition 3. Substitute (3) into (16), we get

$$\begin{aligned}\mathbf{Y}_1 &= \mathbf{F}_{(M-d)}\mathbf{A}\mathbf{F}_Q^T\left(\mathbf{F}_Q^T\right)^*\mathbf{A}^*\left(\mathbf{F}_{(M-d)}\right)^* \\ &\approx Q\mathbf{F}\mathbf{P}\mathbf{F}^*, \\ \mathbf{Y}_2 &= \mathbf{F}_{(M-d)}\mathbf{\Phi}^d\mathbf{A}\mathbf{F}_Q^T\left(\mathbf{F}_Q^T\right)^*\mathbf{A}^*\left(\mathbf{F}_{(M-d)}\right)^* \\ &\approx Q\mathbf{F}\mathbf{\Phi}^d\mathbf{P}\mathbf{F}^*,\end{aligned} \qquad (A.1)$$

where $\mathbf{A}$ is the diagonal matrix defined in (4), $\mathbf{F}_Q^T(\mathbf{F}_Q^T)^*$ approximates an identity matrix up to a multiplicative scalar Q since over intervals of infinite support, cisoids of different frequencies are orthogonal [8]. Thus, the product $\mathbf{A}\mathbf{F}_Q^T(\mathbf{F}_Q^T)^*\mathbf{A}^*/Q$ can be replaced by a diagonal matrix $\mathbf{P}$ with diagonal entries equal to the energy of harmonics, that is, $\mathbf{P} = \text{diag}\,(|a_1|^2, |a_2|^2, \ldots, |a_L|^2)$. Temporarily, we denote $\mathbf{F}_{(M-d)}$ by $\mathbf{F}$ for brevity.

Since $\mathbf{Y}_1$ is a Hermitian matrix and positive-definite, its left and right singular vectors are identical. Let $\boldsymbol{\theta}_\ell$ be the generalized eigenvector corresponding to the generalized eigenvalue ξ_ℓ. According to the definition of the generalized eigen-problem, for the pencil $\boldsymbol{\Lambda}_p - \xi \mathbf{U}_p^* \mathbf{Y}_2 \mathbf{V}_p$, we have

$$\mathbf{U}_p^* \mathbf{F} \mathbf{P} (\mathbf{I} - \xi_\ell \boldsymbol{\Phi}^d) \mathbf{F}^* \mathbf{U}_p \boldsymbol{\theta}_\ell = \mathbf{0}, \tag{A.2}$$

where the expressions of $\mathbf{Y}_1$ and $\mathbf{Y}_2$ in (A.1) are used. Left multiplied by $\boldsymbol{\theta}_\ell^*$, (A.2) becomes

$$(\boldsymbol{\theta}_\ell^* \mathbf{U}_p^* \mathbf{F}) \mathbf{P} (\mathbf{I} - \xi_\ell \boldsymbol{\Phi}^d) (\boldsymbol{\theta}_\ell^* \mathbf{U}_p^* \mathbf{F})^* = 0. \tag{A.3}$$

Since $\mathbf{P}(\mathbf{I} - \xi_\ell \boldsymbol{\Phi}^d)$ is an $L \times L$ diagonal matrix with only the ℓth diagonal element equal to zero, the $1 \times L$ vector $\boldsymbol{\theta}_\ell^* \mathbf{U}_p^* \mathbf{F}$ has the form

$$\boldsymbol{\theta}_\ell^* \mathbf{U}_p^* \mathbf{F} = [0, \ldots, 0, \boldsymbol{\theta}_\ell^* \mathbf{U}_p^* \mathbf{f}(M - d; \omega_\ell), 0, \ldots, 0], \tag{A.4}$$

that is, except for the ℓth element, all others equal zero.

Notice that $\boldsymbol{\Lambda}_p = \mathbf{U}_p^* \mathbf{Y}_1 \mathbf{U}_p$ and $\xi_\ell \boldsymbol{\Phi}^d$ is a diagonal matrix with the ℓth diagonal element equal to one. Hence, (A.3) can be rewritten as

$$\begin{aligned} \boldsymbol{\theta}_\ell^* \boldsymbol{\Lambda}_p \boldsymbol{\theta}_\ell &= (\boldsymbol{\theta}_\ell^* \mathbf{U}_p^* \mathbf{F}) (\mathbf{P} \xi_\ell \boldsymbol{\Phi}^d) (\boldsymbol{\theta}_\ell^* \mathbf{U}_p^* \mathbf{F})^* \\ &= |a_\ell|^2 \, |\boldsymbol{\theta}_\ell^* \mathbf{U}_p^* \mathbf{f}(M - d; \omega_\ell)|^2, \end{aligned} \tag{A.5}$$

which establishes (17). □

ACKNOWLEDGMENTS

NICTA is funded by the Australian Government as represented by the Department of Broadband, Communications and the Digital Economy and the Australian Research Council through the ICT Centre of Excellence program.

REFERENCES

[1] E. A. Homier and R. A. Scholtz, "Rapid acquisition of ultra-wideband signals in the dense multipath channel," in *Proceedings of the IEEE Conference on Ultra Wideband Systems and Technologies (UWBST '02)*, pp. 105–109, Baltimore, Md, USA, May 2002.

[2] V. Lottici, A. D'Andrea, and U. Mengali, "Channel estimation for ultra-wideband communications," *IEEE Journal on Selected Areas in Communications*, vol. 20, no. 9, pp. 1638–1645, 2002.

[3] I. Maravić, J. Kusuma, and M. Vetterli, "Low-sampling rate UWB channel characterization and synchronization," *Journal of Communications and Networks*, vol. 5, no. 4, pp. 319–326, 2003.

[4] A.-J. van der Veen, M. C. Vanderveen, and A. Paulraj, "Joint angle and delay estimation using shift-invariance techniques," *IEEE Transactions on Signal Processing*, vol. 46, no. 2, pp. 405–418, 1998.

[5] A. L. Swindlehurst, "Time delay and spatial signature estimation using known asynchronous signals," *IEEE Transactions on Signal Processing*, vol. 46, no. 2, pp. 449–462, 1998.

[6] B. D. Rao and K. S. Arun, "Model based processing of signals: a state space approach," *Proceedings of the IEEE*, vol. 80, no. 2, pp. 283–309, 1992.

[7] A.-J. van der Veen, E. F. Deprettere, and A. L. Swindlehurst, "Subspace-based signal analysis using singular value decomposition," *Proceedings of the IEEE*, vol. 81, no. 9, pp. 1277–1308, 1993.

[8] R. Roy, A. Paulraj, and T. Kailath, "ESPRIT—a subspace rotation approach to estimation of parameters of cisoids in noise," *IEEE Transactions on Acoustics, Speech, and Signal Processing*, vol. 34, no. 5, pp. 1340–1342, 1986.

[9] R. Roy and T. Kailath, "ESPRIT-estimation of signal parameters via rotational invariance techniques," *IEEE Transactions on Acoustics, Speech, and Signal Processing*, vol. 37, no. 7, pp. 984–995, 1989.

[10] Y. Hua and T. K. Sarkar, "On SVD for estimating generalized eigenvalues of singular matrix pencil in noise," *IEEE Transactions on Signal Processing*, vol. 39, no. 4, pp. 892–900, 1991.

[11] L. L. Scharf and D. W. Tufts, "Rank reduction for modeling stationary signals," *IEEE Transactions on Acoustics, Speech, and Signal Processing*, vol. 35, no. 3, pp. 350–355, 1987.

[12] L. L. Scharf, "The SVD and reduced rank signal processing," *Signal Processing*, vol. 25, no. 2, pp. 113–133, 1991.

[13] L. L. Scharf, *Statistical Signal Processing: Detection, Estimation, and Time Series Analysis*, Addison-Wesley, New York, NY, USA, 1991.

[14] Y. Hua, M. Nikpour, and P. Stoica, "Optimal reduced-rank estimation and filtering," *IEEE Transactions on Signal Processing*, vol. 49, no. 3, pp. 457–469, 2001.

[15] J. Foerster, "Channel modeling sub-committee report final," *IEEE P802.15 Working Group for Wireless Personal Area Networks (WPANs), IEEE P802.15-02/490r1-SG3a*, February 2003.

[16] J. Zhang, R. A. Kennedy, and T. D. Abhayapala, "Cramér-Rao lower bounds for the synchronization of UWB signals," *EURASIP Journal on Applied Signal Processing*, vol. 2005, no. 3, pp. 426–438, 2005.

[17] X.-D. Zhang and Y.-C. Liang, "Prefiltering-based ESPRIT for estimating sinusoidal parameters in non-Gaussian ARMA noise," *IEEE Transactions on Signal Processing*, vol. 43, no. 1, pp. 349–353, 1995.

[18] F. Zhang, *Matrix Theory: Basic Results and Techniques*, Springer, New York, NY, USA, 1999.

[19] G. H. Golub and C. F. V. Loan, *Matrix Computations*, The Johns Hopkins University Press, Baltimore, Md, USA, 3rd edition, 1996.

[20] A. V. Oppenheim and R. W. Schafer, *Discrete-Time Signal Processing*, Prentic-Hall, London, UK, 1989.

[21] D. F. Elliott, Ed., *Handbook of Digital Signal Processing: Engineering Applications*, Academic Press, San Diego, Calif, USA, 1987.